PNAS
www.pnas.org

Supplementary Information for

Fenestrations Control Resting-State Block of a Voltage-Gated Sodium Channel

Tamer M. Gamal El-Din[1*], Michael J. Lenaeus[1*, 2], Ning Zheng[1 †, 3],
William A. Catterall[1, †]

William A. Catterall
Email: wcatt@uw.edu

This PDF file includes:

Supplementary text
Figs. S1
Tables S1
References for SI reference citations

www.pnas.org/cgi/doi/10.1073/pnas.1814928115

Supplementary Information Text

SI Materials and Methods

Drugs. Benzocaine, lidocaine, and flecainide were purchased from Sigma Aldrich.

Molecular Biology. Na_vAb mutants and truncations containing an N-terminal FLAG epitope were constructed by side-directed mutagenesis (QuikChange) and confirmed by sequencing. Recombinant baculovirus was generated by using the Bac-to-Bac system (Invitrogen) and Sf9 (Spodoptera frugiperda) cells.

Protein Expression and Purification. Our procedures were similar to our previous studies (1). *Trichuloplasia ni* cells were cultured on plates and infected with baculovirus encoding the protein of interest. Cells were incubated for 72 h, harvested by pipetting them up from the plate, centrifuging the resulting suspension, and resuspending the pelleted cells into a buffered solution. Cells were subsequently treated with protease inhibitors, weakly sonicated, and the resulting fragments were solubilized with 1% digitonin (EMD Biosciences) for 1 h at 4^{o}C. Lysates were mixed with anti-FLAG resin, incubated for 2 h at 4^{o}C, and the resulting mixture was poured into a chromatography column and washed thoroughly with 0.1% digitonin buffer. Protein was eluted with soluble FLAG epitope at 0.2 mg/mL, then concentrated and further purified by size exclusion chromatography on a Superdex-200 column. The resulting peak fractions were confirmed by SDS-PAGE then combined and concentrated to a concentration of 20 mg/mL. Drugs were added at different times during the purification, with lidocaine added at 10 mM immediately after resuspension and flecainide added at 1mM following size exclusion chromatography.

Crystallization and Data Collection. Our procedures were similar to our previous studies (1). Protein and protein-drug mixtures were reconstituted into 1,2-dimyristoyl-sn-glycero-3-phosphatidylcholine (DMPC):CHAPSO bicelles (Anatrace) that were saturated with drugs at 10 mM (lidocaine) or 1 mM (flecainide) concentrations. The resulting mixtures were mixed with crystallization solutions at a 1:1 ratio and set up as hanging drops over solutions containing 1.8 M ammonium sulfate and 100 mM sodium acetate (pH 5.0-5.4). Crystals appeared within 1-2 weeks. They were cryo-protected with well solution supplemented with drug and increasing concentrations of glucose until a concentration of 28% glucose was reached. Crystals were then harvested in nylon loops and plunged into liquid nitrogen for data collection. Data were collected at Advanced Light Source beam lines bl821 and bl822.

Structure Determination and Refinement. Na_vAb/I217C, Na_vAb/I217C/F203A, and Na_vAb/I217C/F203W were all constructed in the genetic background of Na_VAb/I217C. Flecainide was bound and crystallized with Na_vAb/I217C. Lidocaine was bound and crystallized with Na_vAb/I217C/Δ40.

All data were indexed and scaled with HKL2000 (2) and phased using molecular replacement with Phaser (3). Crystallographic refinement procedures were different for each drug dataset, so they are discussed separately. Na_vAb/I217C, Na_vAb/I217C/F203A and Na_vAb/I217C/F203W data were perfectly twinned, with the twin law k,h,-l in $P2_122_1$ as determined by Xtriage (4). These data were phased with a modified tetramer of Na_vAb/I217C (pdb 3RVY) that did not contain the S6 helix and were subsequently refined by twin refinement with PHENIX (4). We refined XYZ coordinates and individual ADPs/TLS using torsion-angle simulated annealing, NCS restraints, and reference model restraints using voltage sensor residues 1-114 of each 3RVY monomer as a reference template. Reference model restraints were removed after the first cycle of refinement and the S6 helices (including side chains at position 203) were built manually and confirmed with omit maps. NCS restraints were maintained throughout refinement.

The Na_vAb/I217C/Δ40/lidocaine complex data were integrated and scaled with HKL2000 and then processed with PHENIX (4). Na_vAb/I217C/Δ40/lidocaine complex was not twinned per Xtriage (4). The data were phased with a monomer of Na_vAb/I217C (pdb 3RVY), and refined with PHENIX by using torsion-angle simulated annealing and NCS restraints in the early stages of refinement. The lidocaine model in Fig. 1A was manually placed into a fo-fc electron density map calculated from the last round of refinement, but it was not further refined as the binding site was located on a 4-fold crystallographic symmetry axis and lacked sufficient features to identify an appropriate pose. We examined space groups I422, I4, I222 and C2 and ultimately decided upon the space group I4 due to the quality of fit of the electron density maps. Previously published data (pdb 5vb8), which were from the same protein prep as the lidocaine/Na_VAb/I217C/Δ40 structure shown here, were reprocessed into I4 in order to provide an appropriate control.

The data for the Na_vAb/I217C/flecainide complex were integrated and scaled with HKL2000 (2) and processed with PHENIX (4). The Na_vAb/I217C/flecainide data were perfectly twinned, with the twin law –k,-h,-l in $C222_1$, as determined by Xtriage (4). Data were phased with a tetramer of Na_vAb/I217C (pdb 3RVY) and were refined using the twin law –k,-h,-l. We refined XYZ coordinates, individual ADP, and TLS groups using torsion-angle simulated annealing, reference model restraints (voltage sensor residues 1-114 of each 3RVY monomers), and NCS restraints during the early stages of refinement. We examined other space groups (eg., P222 groups, C2) during refinement. Flecainide was manually placed into Fo-Fc maps near the end of refinement, using the shape of the electron density and the expected chemistry of drug binding to find the best fit.

MOLE. Mole figures were calculated using MOLEonline (5). Each figure was calculated within the fenestration by using default parameters, except for a probe radius of 10 Å and interior threshold of 2.0 Å to identify channels able to accommodate the AADs described herein.

Electrophysiology. All measurements were done in *Trichoplusia ni* cells (High5). All Na_vAb constructs used were made on the background of the I217C/N49K mutation to prevent use-dependent slowly

reversible late inactivation (6). All constructs showed good expression, allowing measurement of ionic currents 24–48 h after infection. Whole-cell currents were recorded using an Axopatch 200 amplifier (Molecular Devices) with glass micropipettes (1.5–3.5 MΩ). Capacitance was subtracted and 80–90% of series resistance was compensated using internal amplifier circuitry. Extracellular solution contained in (mM) 140 $NaCl_2$, 2 $CaCl_2$, 2 $MgCl_2$, 10 HEPES, (pH 7.4, adjusted with NaOH). Intracellular solution contained in (mM) 105 CsF, 35 NaCl, 10 HEPES, 10 EGTA, (pH 7.4, adjusted with CsOH). Current–voltage (*I*–*V*) relationships were recorded in response to steps to voltages ranging from -140 to + 50 mV in 10-mV increments from a holding potential of – 140 mV or -160 mV. Conductance-voltage (*G*–*V*) curves were calculated from the corresponding (*I*–*V*) curves. Inhibition curves were fit with the Hill equation. In all experiments, LA or AAD was washed in for two min while the cell was held at HP = -140 mV or -160 mV. The peak current recorded during the first pulse after drug perfusion was taken as a measure of drug inhibition of the resting state. No rundown of Nav current was observed during this incubation period of 2 min used for assessment of resting-state block. In use-dependent experiments, repetitive pulses at 1, 10, and 20 Hz were applied from Vm = -160 mV. Pulses were generated, and currents were recorded using Pulse software controlling an Instrutech ITC18 interface (HEKA). Data were analyzed using Igor Pro 6.2 (WaveMetrics). Dose-response curves were constructed from measuring drug-block of different cells for each drug concentration. Sample sizes were chosen to give s.e.m. values of less than 10% of peak values based on prior experimental experience.

Since fenestrations are the only access pathway at the resting state, their size will determine how easy LAs and AADs reach their receptor in the central cavity. We hypothesized that the shift in drug's potency should correlate with drug's size. We took flecainide as our reference volume/size and we refer to the change in size of other drugs as a percentage of flecainide volume $V_{drug}/V_{flecainide}$. To estimate the shift of dose-response curve, we multiply the ratio of molecular volumes of drug/flecainide by the shift in IC50 caused by the mutant in case of flecainide. We estimated the change in drug's IC50 from this equation:

$$\Delta\mathrm{IC50(mutant)}_{drug} = \frac{V_{drug}}{V_{flecainide}} \times \Delta\mathrm{IC50(mutant)}_{flecainide}$$

SI Discussion

Effects of Rotamer Conformations at Position 203. Crystal structures are static, whereas functional proteins are dynamic. We wondered what the impact of different rotamer conformations at the position of F203 would be. Inspection of our different crystal structures of Na_VAb/WT and Na_VAb/F203W revealed different rotamer conformations. Our crystal structure of Na_vAb/F203W showed a complete block of the fenestration by a "down" rotamer, but an "up" rotamer present in other subunits showed only partial block (Fig. 2). Based on our functional data, we speculate that the fenestrations are transiently blocked by the sidechain of W203, depending its rotamer conformation, which results in a partial reduction rather than a complete block of drug access. In our crystal structures, three of the four

subunits have the down rotamer, which blocks the fenestration, consistent with our electrophysiological data showing that resting-state block is substantially reduced but not eliminated. Changes in the size of the fenestrations have also been reported in different channel states by comparing X-ray crystallographic studies of pre-open and inactivated states of Na_VAb (7, 8) and by comparing cryo-EM structures of different domains in $Na_v1.4$ and Na_vPas eukaryotic channels (9, 10). Overall, these comparisons indicate that the size and shape of the fenestrations are likely to be dynamic and exert control over drug access in a complex way during the functional cycle of a Na_V channel.

Functional Properties of Receptor Site and Fenestration Mutants. Mutation of T206 in the LA/AAD receptor site to alanine (Na_VAb/T206A) slowed inactivation and shifted the voltage dependence of channel gating as described (11). We analyzed the functional properties of the fenestration mutants Na_VAb/F203A and Na_VAb/F203W using whole-cell voltage clamp methods as described in the main text and in SI Methods. The current-voltage (I/V) relationships and the voltage dependence of activation (G/V) relationships for both mutants were similar to Na_VAb/WT (Fig. S1A, B). Although the mutations did not cause any changes in the activation profile, there were significant shifts in the voltage dependence of inactivation. Namely, the F203W mutation shifts the voltage dependence of inactivation 45-mV to more positive membrane potentials, while the F203A mutation caused a 22-mV negative shift (Fig. S1C, D). Our experiments are designed to target the resting state of Na_VAb by allowing drug binding only at a negative holding potential (-140 mV or -160 mV) at which none of these Na_VAb constructs are detectably inactivated. Therefore, our experiments measure resting-state block with little or no contribution from open-state block or channel inactivation.

Drug Protonation in Local Anesthetic and Antiarrhythmic Drug Action. LA's and AAD's are secondary or tertiary amines that can be reversibly protonated and deprotonated in aqueous solution at physiological pH. The active form of these drugs is the positively charged, protonated amine (12). The uncharged, deprotonated forms of the drugs are thought to diffuse through the membrane. For open-state block, these uncharged amines may re-protonate in the cytosol or in the central cavity of the pore before binding to their receptor site. For resting-state block, re-protonation is thought to take place in the central cavity, which has sufficient water and protons to support this process. Although the drugs we have studied differ in pKa (flecainide, 9.3; lidocaine, 7.7; and benzocaine, 2.7), diffusion through the membrane and re-protonation in the central cavity are much faster processes than diffusion through the narrow fenestrations and binding to the small drug receptor site; therefore, membbrane diffusion and protonation are unlikely to be rate-limiting for resting-state block. Consistent with this expectation, flecainide is the most highly charged drug and therefore should diffuse through the membrane most slowly, yet flecainide is the most effective of these three drugs drug in resting-state block.

Potential Clinical Significance of Differential Binding of Lidocaine and Flecainide. In both experimental and clinical settings, block of sodium channels by lidocaine and other Class IB AADs is

more rapidly reversible than block by flecainide and other Class IC AADs (13, 14). Because of this difference in the kinetics of drug dissociation, drug block accumulates during repeated action potentials and reduces the Vmax of the action potential for flecainide and other Class IC drugs but not for lidocaine and other Class IB drugs at therapeutic doses (15). These differences in the kinetics of drug dissociation and the cumulative effects on Vmax are thought to be responsible for the difference in clinical uses of these drugs. Lidocaine and other Class 1B AADs are used only for ventricular arrhythmias, whereas flecainide and other Class IC AADs are used primarily for atrial arrhythmias and are contraindicated for patients with ventricular dysfunction. The differences in binding poses that we have observed for lidocaine and flecainide may contribute to the difference in drug dissociation observed in experimental studies and in the clinic. We have observed that lidocaine binds in the center of the central cavity and makes limited interactions with its walls. In contrast, flecainide extends its larger hydrophobic moieties toward the walls of the cavity and makes additional hydrophobic interactions there. If these drugs bind similarly to human $Na_V1.5$ channels, these additional hydrophobic interactions may stabilize the drug-receptor complex and make dissociation of flecainide and other Class IC drug comparatively slow.

Potential Clinical Impact of Drug Entry Through Fenestrations. Our results reveal that resting state block of Na_VAb is mediated by drug entry through fenestrations. The balance of open-state block through the open activation gate vs. resting-state block of closed channels is an important determinant of the clinical efficacy of LAs and AADs. Both of these drug classes block sodium channels more effectively in rapidly firing cells, which allows relief of pain and prevention of arrhythmias without loss of sensation or cardiac function. If similar mechanisms control drug entry to the LA/AAD receptor site in human sodium channels, drug entry through fenestrations would be a key determinant of use-dependent drug action that is essential for effective and safe use of these drugs.

Unlike Na_VAb, eukaryotic sodium channels are composed of four homologous, but non-identical, domains in a single polypeptide (16). The amino acid sequences, structures, and shapes of the fenestrations are different in the four domains in cryo-electron microscopic structural models of eukaryotic sodium channels (10). Moreover, fenestrations change size and shape in different functional states of sodium channels (8). Therefore, it is likely that the fenestrations play complex, dynamic roles in providing drug access in closed states of sodium channels. It is important to follow up this work with similar structural and functional studies of eukaryotic sodium channels; however, these studies will be difficult because different mutations must be inserted in each of the four domains and their effects on overall drug block cannot be easily separated.

Potential Impact of Fenestrations in Ion Channel Drug Discovery. Our results show that changes in drug size can determine the level of resting-state block and thereby determine the extent of frequency-dependent block. Therefore, in future drug discovery, the chemical structure of drugs can be fine-tuned to fit the drug receptor site, as in current medicinal chemistry, and both drug size and drug shape can

be adjusted to give optimum resting-state block and the desired level of frequency-dependent block. We speculate that small drugs and long, narrow drugs will be more effective in passing through the fenestrations and causing resting-state block, whereas more bulky drug molecules will give weak resting-state block and a greater ratio of frequency-dependent block. Fine-tuning the ratio of open-state to resting-state block for LAs, AADs, and other classes of sodium channel blocking drugs will give unprecedented flexibility and specificity for next-generation drug discovery. Fenestrations have also been observed in the structures of potassium channels (17). They can be modified by co-expression of an auxiliary subunit, KCNE1, and they can serve as drug receptor sites (17). These studies substantially broaden the pharmacological significance of fenestrations to potassium channels and potentially other ion channels as well.

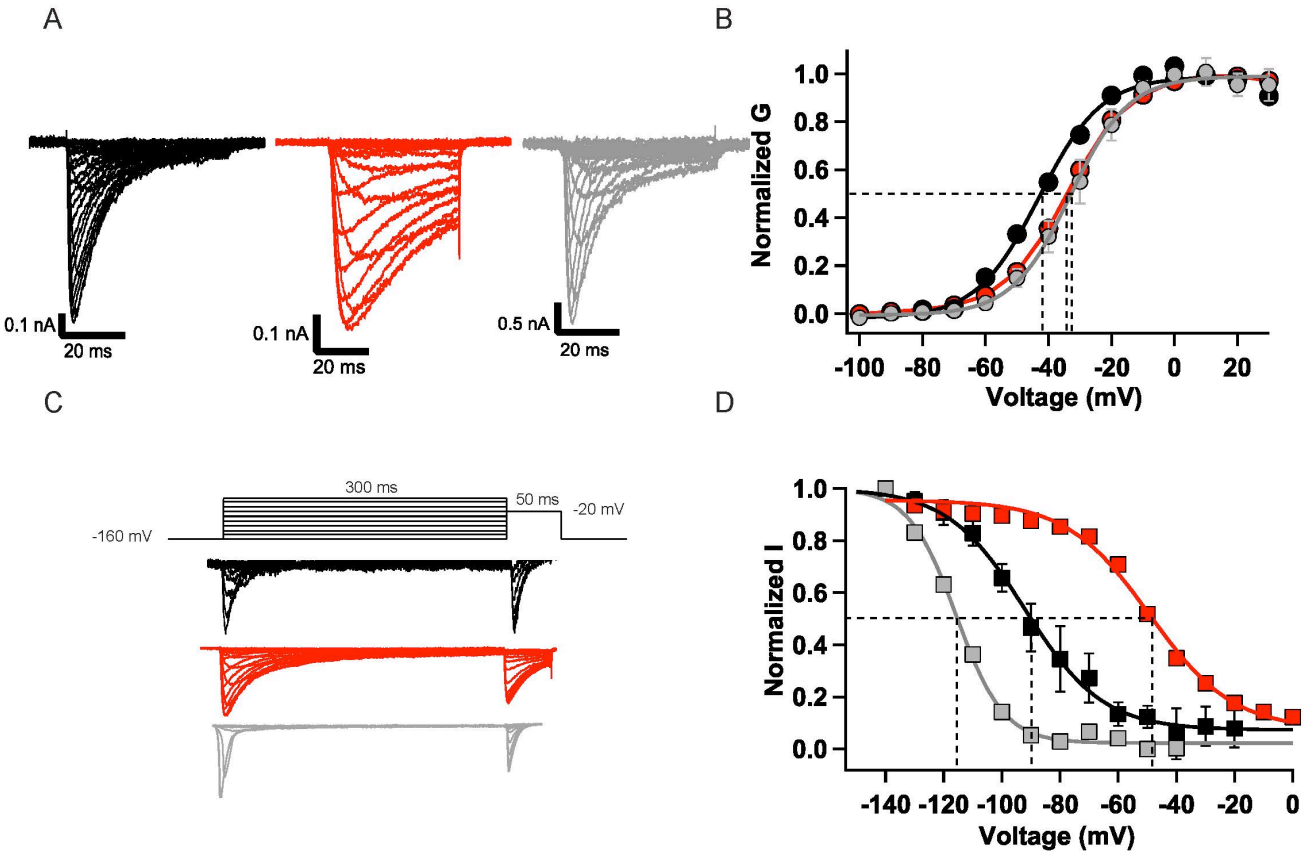

Figure S1. Biophysical properties of fenestration mutants A. Na_vAb/WT (black) and Na_vAb/F203W (red) and Na_vAb/F203A (gray) currents in response to depolarizations to potentials ranging from -100 mV to +50 mV in 10 mV steps. **B.** Conductance-voltage relationships for Na_vAb/WT (black) and Na_vAb/F203W (red) and Na_vAb/F203A (gray). The lines through the curves are fits of Boltzmann relationships with $V_{1/2}$ values of -43 ± 0.2 mV, k= 9.9 ± 1.4 for Na_vAb/WT, -34.3 ± 0.2 mV, k= 9.95 ± 0.3 for Na_vAb/F203W, and -33 ± 0.5 mV, k= 9.3 ± 0.5 for Na_vAb/F203A. **C, D.** Voltage-dependence of inactivation for Na_vAb/WT (black), Na_vAb/F203W (red) and Na_vAb/F203A (gray) by depolarizations to -20 mV after 300-ms conditioning prepulses to the indicated potentials. Na_vAb/WT (black, -93 ± 3 mV), Na_vAb/F203W (red, -48 ± 2 mV) Na_vAb/F203A (gray, -115 ± 2 mV).

Table S1. X-ray Crystallography Statistics

	Na_vAb I217Cd40, +Lidocaine	Na_vAbI217C + Flecainide	Na_vAb I217C/F203A	Na_vAb I217C/F203W
DATA COLLECTION				
Space group	I 4	$C222_1$	$P2_122_1$	$P2_122_1$
Unit cell	126.596 126.596 192.219 90 90 90	177.525 177.687 192.923 90 90 90	125.782 125.969 192.299 90 90 90	126.22 126.09 192.88 90 90 90
Resolution	3.00 Å	3.455 Å	2.90 Å	3.20 Å
Rmerge	0.120 (>1)	0.157 (>1)	0.138 (>1)	0.186 (>1)
I/oI	24 (0.9)	8.75 (0.9)	15.2 (1.5)	9.6 (1.3)
Completeness (%)	100 (99.4)	99.9 (98.8)	100 (99.9)	100.0 (100)
Redundancy	16.3 (9.4)	6.3 (5.8)	7.0 (6.8)	7.3 (7.5)
CC ½ (highest shell)	0.657	0.431	0.580	0.283
REFINEMENT				
Resolution	29.84 – 3.002 (3.109 – 3.002)	29.86 – 3.455 (3.579 – 3.4555)	29.93 - 2.90 (3.004 – 2.9)	29.96 - 3.198 (3.312-3.198)
No. of Reflections	30052 (2887)	39868 (3833)	68271 (6746)	51427 (4990)
R_{work}/R_{free}	0.1931/0.2296	0.2335/0.2864	0.21170.2568	0.2286/0.2653
No. atoms	3949	7041	7494	7534
Protein	3645	6957	7268	7158
Ligand/Ion	263	84	226	376
Water	41	0	0	0
B-factor	85.15	131.30	84.70	82.0
Protein	113.80	131.20	85.10	82.4
Ligand/Ion	123.10	134.90	73.50	74.30
Water	95.80	-	-	61.01
R.m.s. deviations				
Bond lengths (Å)	0.008	0.012	0.011	0.011
Bond angles (degrees)	1.32	1.67	1.44	1.49

SI References

1. Lenaeus MJ*, et al.* (2017) Structures of closed and open states of a voltage-gated sodium channel. *Proc Natl Acad Sci U S A* 114(15):E3051-E3060.
2. Otwinowski Z & Minor W (1997) Processing of X-ray diffraction data collected in oscillation mode. *Methods Enzymol* 276:307-326.
3. McCoy AJ*, et al.* (2007) Phaser crystallographic software. *J Appl Crystallogr* 40(Pt 4):658-674.
4. Adams PD*, et al.* (2010) PHENIX: a comprehensive Python-based system for macromolecular structure solution. *Acta Crystallogr D Biol Crystallogr* 66(Pt 2):213-221.
5. Berka K*, et al.* (2012) MOLEonline 2.0: interactive web-based analysis of biomacromolecular channels. *Nucleic Acids Res* 40(Web Server issue):W222-227.
6. Gamal El-Din TM, Martinez GQ, Payandeh J, Scheuer T, & Catterall WA (2013) A gating charge interaction required for late slow inactivation of the bacterial sodium channel NavAb. *J Gen Physiol* 142(3):181-190.
7. Payandeh J, Scheuer T, Zheng N, & Catterall WA (2011) The crystal structure of a voltage-gated sodium channel. *Nature* 475(7356):353-358.
8. Payandeh J, Gamal El-Din TM, Scheuer T, Zheng N, & Catterall WA (2012) Crystal structure of a voltage-gated sodium channel in two potentially inactivated states. *Nature* 486 135-139.
9. Shen H*, et al.* (2017) Structure of a eukaryotic voltage-gated sodium channel at near-atomic resolution. *Science*.
10. Yan Z*, et al.* (2017) Structure of the Nav1.4-beta1 complex from electric eel. *Cell* 170(3):470-482 e411.
11. Gamal El-Din TM, Lenaeus MJ, Ramanadane K, Zheng N, & Catterall WA (2018) *J Gen Physiol* (In press)
12. Hille B (1977) Local anesthetics: hydrophilic and hydrophobic pathways for the drug-receptor reaction. *J. Gen. Physiol.* 69:497-515.
13. Ragsdale DS, Scheuer T, & Catterall WA (1991) Frequency and voltage-dependent inhibition of type IIA Na+ channels, expressed in a mammalian cell line, by local anesthetic, antiarrhythmic, and anticonvulsant drugs. *Mol.Pharmacol.* 40:756-765.
14. Ramos E & O'Leary M E (2004) State-dependent trapping of flecainide in the cardiac sodium channel. *J Physiol* 560(Pt 1):37-49.
15. Wang Z, Pelletier LC, Talajic M, & Nattel S (1990) Effects of Flecainide and Quinidine on Human Atrial Action-Potentials - Role of Rate-Dependence and Comparison with Guinea-Pig, Rabbit, and Dog-Tissues. *Circulation* 82(1):274-283.
16. Gamal El-Din TM, Lenaeus MJ, & Catterall WA (2017) Structural and Functional Analysis of Sodium Channels Viewed from an Evolutionary Perspective. *Handb Exp Pharmacol*.
17. Wrobel E*, et al.* (2016) KCNE1 induces fenestration in the Kv7.1/KCNE1 channel complex that allows for highly specific pharmacological targeting. *Nat Commun* 7:12795.